ELSEVIER

Contents lists available at ScienceDirect

### Electrochimica Acta

journal homepage: www.journals.elsevier.com/electrochimica-acta





# Revealing the impact of surface composition of electrodeposited Cu and Ni nanoparticles on the specific electrooxidation of uric acid

E.V. Butyrskaya <sup>a</sup>, N. Korkmaz <sup>b</sup>, E.V. Zolotukhina <sup>c</sup>, S.A. Kleinikova <sup>c</sup>, M. Koch <sup>d</sup>, Y.E. Silina <sup>e,\*</sup>

- a Voronezh State University, Department of Analytical Chemistry, Voronezh, Russia
- <sup>b</sup> KIST Europe AI Convergence Cluster, Korea Institute of Science and Technology, Saarbrücken, Germany
- <sup>c</sup> Federal Research Center of Problems of Chemical Physics and Medicinal Chemistry, Russian Academy of Sciences, Moscow region, Russia
- <sup>d</sup> HTW saar University of Applied Sciences, Saarbrücken, Germany
- e Saarland University, Department of Biochemistry, Saarbrücken, Germany

#### ARTICLE INFO

Keywords:
Electrodeposited nanoparticles (NPs)
Defect oxides
Specificity
Electrooxidation of uric acid

#### ABSTRACT

The electrodeposition of transition metal nanoparticles (NPs) enables the formation of structures with complex surface chemistry and enhanced catalytic properties. However, their electrocatalytic behavior can differ significantly from that of NPs synthesized by other methods, due to the formation of defect oxides, hydroxides, and distinct interactions with molecular oxygen. This study investigates the role of uric acid (UA) polarizability during complexation with catalytic centers of electrodeposited copper (Cu-NPs) and nickel (Ni-NPs) nanoparticles both containing surface defect oxides and the influence of molecular oxygen on UA detection under alkaline conditions. The results show that although Cu-NPs exhibit higher sensitivity toward UA, this is accompanied by reduced specificity due to side interactions with oxygen. In contrast, Ni-NPs enhance UA polarizability without engaging in oxygen interactions, leading to more specific UA electrooxidation. These findings offer insight into the design of electrodeposited electrocatalysts with tailored specificity for UA detection.

#### 1. Introduction

The role of electrodeposition of transition metals on properties of nanostructured catalysts has been summarized with a focus on fuel cells, water splitting, and carbon dioxide electroreduction applications [1–3]. The preparation of catalysts through electrodeposition offers numerous advantages, including the controlled formation of a catalytic layer by adjusting electrodeposition parameters (such as current, time, and layer thickness), strong binding between the electrocatalyst and electrode, simplicity in operation, the ability to form not only continuous layers but also nanoparticulate films with tunable surface chemistry and properties [4–6]. Additionally, electrodeposited nanoparticles (NPs) of transition metals can be produced in both, *e.g.*, highly monodisperse and polydisperse state [7], exhibit enhanced electroanalytical performance in oxygen reduction and hydrogen evolution reactions [3,8], as well as improved electrocatalytic stability and limited aggregation [9].

It is believed that the advanced electrochemical properties of electrodeposited NPs of transition metals may be linked to their numerous

structural defects [10], which influence their catalytic activity and, consequently, their electroanalytical performance [11].

Cation and oxygen vacancies have been reported as types of structural defects present in electrodeposited NPs [12–14]. Notably, altering the type, amount and ratio of defect oxides in electrodeposited NPs can induce structural rearrangements in the crystals, create new active sites, promote the adsorption of catalytic reaction intermediates, and thus affect the kinetics of RedOx reactions [15,16].

Recently, it has been shown that electrodeposited copper nanoparticles (Cu-NPs), in the presence of molecular oxygen, exhibit copper (II)-induced oxidation (catalytic effect) in RedOx reactions with uric acid (UA) [17]. More importantly, it was demonstrated that the increase of defect oxides and  $\text{Cu}^+/\text{Cu}^{2+}$ -catalytic centers after heating of electrodes at 70 °C for 30 min leads to an increase of [Cu<sup>+</sup>(UA)] and [Cu<sup>2+</sup>(UA)<sub>n</sub>] complexes, which are responsible for the specific UA determination in complex fermentation media [17]. In other words, the presence of defect oxides on the surface of electrodeposited Cu-NPs can ultimately influence the reaction pathways with the target analyte, such

<sup>\*</sup> Corresponding author at: Institute of Biochemistry, Saarland University, Saarbrücken, Campus B 2.2, room 317, Germany. E-mail addresses: yuliya.silina@uni-saarland.de, yuliya.silina@gmx.de (Y.E. Silina).

as IIA

UA – is an important physiological biomarker, and its non-enzymatic analysis in real samples (*e.g.*, fermentation samples, human urine, etc.) with high specificity is an actual electroanalytical task. However, to the best of our knowledge, only a few studies have been conducted on the development of specific non-enzymatic electrochemical sensors for UA determination in the presence of interfering electroactive species.

Most of the proposed sensing layer designs for UA determination rely on the use of oxides of lanthanides and transmission metals, for example, gadolinium oxide,  $Gd_2O_3$  [18], copper oxide, CuO [19], or cobalt oxide,  $Co_3O_4$  [20]. Although the importance of electrodeposited defect oxides in the specificity of UA analysis was recently highlighted [17], the reasons why electrodes based on defect oxides of transition metals, even those of similar nature, may exhibit different specificities in the same RedOx reactions remain unclear.

In this study, the specificity of electrooxidation of uric acid (UA) on the surface of electrodes modified with electrodeposited NPs (copper, Cu-NPs, and nickel, Ni-NPs, as case study) was investigated both in the presence and absence of oxygen. Briefly, the specificity of electrodes tends to depend on the polarization ability of UA in the presence of catalytic centres (Cu<sup>+</sup>, Cu<sup>2+</sup>, Ni<sup>2+</sup>, Ni<sup>3+</sup>) represented by defect oxides of electrodeposited NPs (*i*) and the adsorption of molecular oxygen (*ii*). More significantly, different interaction behaviour of molecular oxygen was observed depending on the surface chemistry of electrodeposited NPs (*iii*). At the same time, different interaction between molecular oxygen and surface chemistry of electrodeposited NPs affected the type of reaction products formed during electrooxidation of UA in alkaline solutions (*iv*).

A deeper understanding of the impact of surface chemistry of electrodeposited NPs on their electrocatalytic properties could lead to significant advances in electrochemical sensors e.g., creating electrodes with tailored functionality and specificity in the future.

#### 2. Experimental part

#### 2.1. Chemicals and materials

CuSO<sub>4</sub>, NiSO<sub>4</sub>, uric acid (UA), KOH, ascorbic acid, ethanol (EtOH), glycerol, ethylamine, ethanol amine, urea, hydrazine solution ((N<sub>2</sub>H<sub>4</sub>), 35 wt. % in H<sub>2</sub>O), Pd wire (99.99 %) used as an anode, HCIO<sub>4</sub>, (PbNO<sub>3</sub>)<sub>2</sub>, derivatization agent N-Trimethylsilyl-N-methyl trifluoroacetamide (MSTFA), n-hexane were obtained from Merck (Darmstadt, Germany). Oxygen-free standard solution (OXCAL for deoxygenation, 0 % O<sub>2</sub>) was received from (Pyro Science GmbH, Aachen, Germany).

Screen printed electrodes (SPEs) produced on ceramic substrates and modified by graphene oxide (DPR-110RGPHOX) were purchased from DropSens (Metrohm, Germany). For buffer, stock and standard solutions preparation, de-ionized water (DI) generated by an Elga PureLab (Celle, Germany) water purification system was used.

#### 2.2. Preparation of electrodes modified with electrodeposited NPs

To systemize the influence of defect oxides, present on the surface of electrodeposited NPs on the specificity of UA electrooxidation, it is necessary to synthesize NPs with similar physicochemical properties (e. g., Ni-NPs and Cu-NPs) and compare their performance.

For this goal, Cu-NPs were electrodeposited onto the surface of SPEs from 30 mM CuSO<sub>4</sub> solution at -0.5 mA for 30 s. Briefly, 10  $\mu$ L of the CuSO<sub>4</sub> electrolyte was placed on the working electrode of the SPE, followed by cathodic electrodeposition. A Pd-wire was used as the anode. To increase the electrode area covered with electrodeposited NPs, the procedure was repeated three times, each time with a fresh droplet of electrolyte. The resulting electrodes were used without any additional pre-treatment steps.

The same electrodeposition protocol was used to prepare Ni-NPs. To this end,  $30\ mM\ NiSO_4$  electrolyte was used. After the Cu-NPs and Ni-

NPs layers were formed, the electrodes were carefully washed with DIwater, dried and stored under ambient conditions.

#### 2.3. Electrochemical studies

The produced electrodes were tested in cyclic voltammetry (CV) at a scan rate of 50 mV/s, spanning a potential range from -0.4~V to 0.4~V, on a one-channel PalmSens4 potentiostat (PalmSens, Utrecht, The Netherlands). For this goal,  $150~\mu L$  of either background electrolyte or model UA solution was dropped onto the surface of all three electrodes (counter, reference, and working electrodes). The specificity of electrodes modified with Cu-NPs or Ni-NPs was assessed in amperometric (AM) mode at 0.22~V and 0.15~V vs. silver oxide electrodes, respectively.

Electrodes modified with electrodeposited NPs were calibrated in multi-step amperometric mode (MAM) [21]. Calibration was performed using external standards at alkaline pH. The pH of background electrolytes, stocks, and calibrants was monitored with a Horiba LAQUAtwin pH meter (pH-22) (Neomeris, France).

# 2.4. Evaluation of electroactive surface area (ECSA) of electrodes with electrodeposited NPs

To estimate the ECSA of electrodes modified with electrodeposited Cu-NPs, the earlier reported protocol using 0.01 M HClO<sub>4</sub> and 1 mM PbCl<sub>2</sub> electrolyte was applied [22]. The experiments were conducted under an argon atmosphere. The lead desorption peak charge (from (PbNO<sub>3</sub>)<sub>2</sub> solution in HClO<sub>4</sub>) was used to determine the surface area of Cu-NPs. The ECSA of Cu-NPs, defined at E=-0.36 V, was 0.021±0.003 cm<sup>2</sup>

The ECSA evaluation of Ni-NPs deposited on the surface of SPEs was conducted according to protocol reported in [23], based on the Ni(OH) $_2$  oxidation peak at alkaline pH. The calculated ECSA of Ni-NPs was 0.12  $\pm 0.03~\text{cm}^2$ .

### 2.5. Scanning electron microscopy (SEM) and energy dispersive X-ray (EDX) studies

The morphology of Cu-NPs and Ni-NPs electrodeposited on the surface of SPEs was studied using an FEI Quanta 250 FEG SEM (FEI Company, USA) operated at 10 kV in high vacuum.

SEM/EDX analysis was performed using a JEOL JSM-6460LV and an Oxford INCA 4.13 X-Ray spectrometer at 15 kV accelerating voltage in high vacuum.

#### 2.6. Atomic force microscopy (AFM)

To access the surface texture of ED NPs, AFM investigations of the formed electrodes modified with Cu-NPs and Ni-NPs, were conducted on a PARK NX 10 AFM system (Park Systems, South Korea). All measurements were performed in non-contact scanning mode under ambient conditions. Mounted AFM ACTA (NCHR) probes compatible with Park NX 10 were purchased from Schaefer Technologie GmbH (Germany).

Images were recorded with a scan size of 5  $\mu m$  x 5  $\mu m$  and with a resolution of 512 pxl x 512 pxl. Average roughness (Ra) and surface root mean square roughness (Rq) values were extracted from three AFM images for each sample using the Gwyddion image processing software (http://gwyddion.net/) and calculated as the mean roughness  $\pm$  standard deviation.

# 2.7. RAMAN spectroscopy characterization of the surface of electrodeposited NPs

To analyze the surface chemistry of the electrodeposited NPs, RAMAN spectroscopy was performed using a LabRAM HR Evolution HORIBA equipped with a 633 nm He-Ne laser (Melles Griot, IDEX Optics and Photonics, Albuquerque, NM, USA). The *G*-band of the carbon

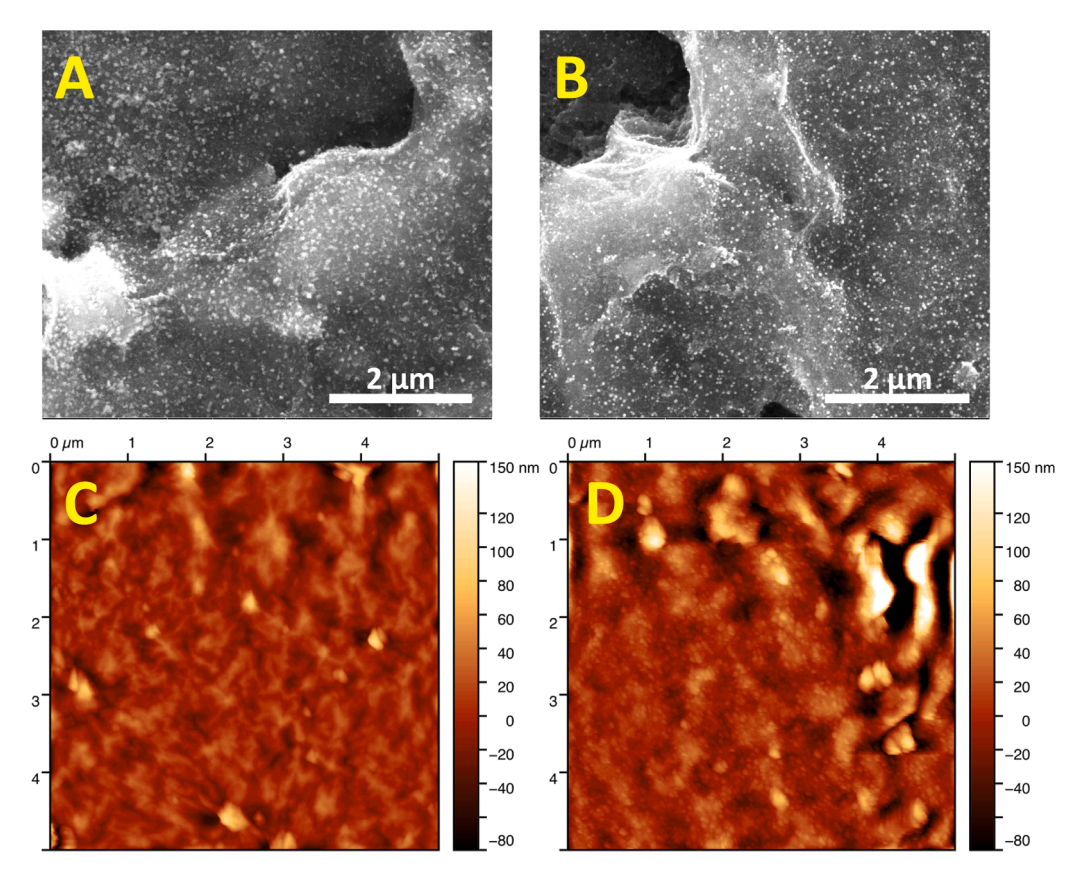


Fig. 1. SEM (A,B) and AFM (C,D) images of electrodes modified with electrodeposited Cu-NPs (A,C) and Ni-NPs (B,D).

template (material of the working electrode of the SPEs, graphene oxide) was used for scaling of the signal intensities.

### 2.8. Oxygen mini-sensor studies

To reveal the impact of dissolved oxygen content ( $\mu$ mol·L·¹) on the results of UA electrooxidation, an OXR430 optical needle oxygen minisensor (PyroScience GmbH, Aachen, Germany) was used. The signal read-outs were taken under ambient conditions (21 % or 270  $\mu$ mol/L dissolved oxygen) in a 150  $\mu$ L droplet of test solution placed on the surface of SPEs modified with electrodeposited NPs, while simultaneously starting CV.

To model an oxygen-free environment (0 % or 0 µmol/L dissolved oxygen content), UA test solutions were prepared in OXCAL for deoxygenation maintaining an alkaline pH of 9.0  $\pm$  0.2. The results obtained in this oxygen-free environment were compared to those recorded for solutions prepared in the background electrolyte (21 % or 270 µmol/L) and tested under ambient conditions.

#### 2.9. Computational modeling

The calculations were performed using Gaussian09 program with the B3LYP/6–311 + G (d,p) method for all atoms. The role of a solvent (water) was counted by PCM. Although, according to the literature, UA exists in solution up to pH 9.8 in a form of a mono-anion [24], in some cases, at alkaline pH, the elongation of the C=N bond may cause the mono-anion to become thermodynamically unstable [25]. Therefore, in our calculations, we considered both forms UA, e.g., the mono- and di-anions.

The change in the total charge on the atoms of mono- and di-anions of UA upon the simultaneous attachment of molecular oxygen and metal atoms (or ions) was also examined by analyzing the atomic charges using the Malliken method. The calculation was performed using the

previously proposed methodology [26].

#### 2.10. Gas chromatography mass spectrometry (GC-MS)

To compare the end-products formed during the electrooxidation of UA on the surface of electrodeposited Cu-NPs and Ni-NPs, GC–MS analysis was performed. For this goal, a 150  $\mu L$  droplet of 2 mM UA (pH 9.0  $\pm$  0.2) was placed on Cu-NPs and Ni-NPs modified electrodes, followed by microelectrolysis conducted at 0.2 V for 3600 s. The aqueous phase of the collected droplets was then evaporated under a nitrogen atmosphere, and derivatization was carried out using 60  $\mu L$  of MSTFA reagent. The resulting suspension was heated at 60  $^{\circ} C$  for 30 min. Finally, the samples were diluted in a ratio of 1:10 with n-hexane and injected into the GC–MS system (LECO Pegasus HT-C, Agilent).

To identify the characteristic peaks associated with the electrocatalytic oxidation products of UA, a blank reference sample containing 2 mM UA (not exposed to the electrodes) was subjected to the same pretreatment protocol.

Chromatographic separation was performed using a Phenomenex Zebron ZB-35HT column (30  $m \times 0.25$  mm, film thickness 0.25  $\mu m$ ) with the following temperature gradient: starting temperature was 50 °C held for 5 min, raised to 340 °C held for 15 min. Ionization was carried out at 70 eV (electron impact, EI), and mass spectra were recorded in the m/z range of 40 – 400.

#### 3. Results and discussion

# 3.1. Characterization of electrodes modified with electrodeposited Cu-NPs and Ni-NPs

The specificity of catalytic electrooxidation refers to a catalyst's ability to selectively oxidize a target analyte or chemical species, as opposed to other electroactive molecules. Importantly, at the

**Table 1**Summary of RAMAN characteristic bands obtained from the studied electrodes modified with electrodeposited Cu-NPs and Ni-NPs.

Electrodeposited NPs	Characteristic peaks, cm <sup>-1</sup> *	Corresponding form
Cu-NPs	87, 145, 221, 417, 528	Cu <sub>2</sub> O
$(Cu_2O_x (x \leq 1))$	296, 347, 396, 612	CuO
	195, 221, 483, 579, 633	$Cu_4O_3$
Ni-NPs	294/325, 450,770, 850-853	γ-NiOOH
(NiO <sub>x</sub> )	450, 540, 580–589	Ni-O
	560, 610-611, 667	NiOOH

<sup>\*</sup> for data interpretation and validation following literature was used (for Cuoxides) and (for Ni-oxides) [32–38].

maintained constant electrochemical operation conditions namely the design, *viz.* the structure and surface composition of the electrode determine its electrocatalytic activity and specificity of electrocatalysis.

SEM analysis of the surface of electrodeposited copper and nickel layers, prepared using the same electrodeposition protocol (*see Experiment*), revealed their similar morphology (Fig. 1A,B). Electrodeposited metallic nanoparticles (NPs) appeared as high-contrast whitish spots distributed across the surface of the graphene oxide (Fig. 1A,B). The size of the electrodeposited NPs ranged from 30 to 50 nm (ESI, Fig S1).

EDX analysis confirmed the presence of copper and nickel on the surface of SPEs formed during electrodeposition, **ESI**, **Fig. S2**. Despite having a very similar surface morphology at first glance, as observed via SEM (**Fig. 1A**,**B**), the topography of Cu-NPs and Ni-NPs slightly differed (**Fig. 1C**,**D**). Specifically, the mean roughness values extracted from the AFM topography data for Ni-NPs were nearly twice as high compared to Cu-NPs, **ESI**, **Fig. S3**. This trend was consistent with the ECSA of the electrodes, which was  $0.021\pm0.003~\text{cm}^2$  for Cu-NPs and  $0.12\pm0.03~\text{cm}^2$  for Ni-NPs.

Nanoparticles (NPs) of transition metals produced via electrodeposition have been reported to exhibit various defect structures, such as non-stoichiometric oxides. These defects play a crucial role in enhancing the electrochemical activity of the NPs. Therefore, to investigate the surface chemistry of the electrodeposited Cu-NPs and Ni-NPs, and to confirm the presence of surface defects, particularly non-stoichiometric oxides, RAMAN spectroscopy was employed [5,17]. RAMAN investigations of the synthesized NPs confirmed that electrodeposition was accompanied by the formation of non-stoichiometric defect oxides of copper and nickel, Table 1 (see also ESI, Fig. S4). The non-stoichiometric composition of copper [27–31] and nickel [32–38] with oxygen results in lattice and/or surface defects.

In most defect metal oxides, metal ions exist in an ionic state, meaning they are positively charged cations (metal ions) and negatively charged oxide anions, held together by electrostatic force. In terms of electrocatalysis, the presence of defect oxides on the surface of electrodeposited nanoparticles (NPs) and the appearance of new catalytic centres can alter their interaction with a target analyte and oxygen, compared to pathways observed for NPs composed solely of atoms. In other words, the presence of catalytic centres, represented by  $\mathrm{Cu^+}$ ,  $\mathrm{Cu^{2+}}$ ,  $\mathrm{Ni^{2+}}$ ,  $\mathrm{Ni^{3+}}$  on the surface of electrodeposited Cu-NPs and Ni-NPs, can be expected.

Notably, in addition to defect oxides, the surface of Ni-NPs also contained hydroxides (Table 1), which can significantly influence the electronic structure of NiO [39,40]. Thus,  $\gamma$ -NiOOH, also known as nickel oxyhydroxide, is a complex nickel oxide with a distinct crystal structure and specific properties [32–38]. Along with prominent peaks corresponding to NiO,  $\gamma$ -NiOOH, and NiOOH, a weak peak at 665 – 667 cm<sup>-1</sup>, indicating the presence of defect Ni<sup>3+</sup>, was detected on the surface of Ni-NPs (**ESI**, **Fig. S4**).

In summary, the defect-rich surface chemistry of Ni-NPs, combined with a more pronounced oxide-to-hydroxide conversion, may enhance their electrocatalytic activity compared to Cu-NPs (*see below*).

**Table 2**Electroanalytical performance of electrodes with electrodeposited NPs in model UA solutions at pH 9.

Electrode	Calibration formula in model solutions*	R <sup>2</sup>	Sensitivity**  µA·µM <sup>-</sup> 1·cm- <sup>2</sup>	LDR, μM
Cu-NPs	$y = 0.0064 \cdot x + 0.185$	0.9965	0.304	0 – 100
	$y = 0.0054 \cdot x + 0.161$	0.9965	0.257	100 – 400
	$y = 0.0053 \cdot x + 0.174$	0.9995	0.252	100 – 2000
Ni-NPs	$y = 0.0046 \cdot x + 0.040$	0.9995	0.038	0 - 100
	$y = 0.0038 \cdot x + 0.188$	0.9873	0.031	100 – 400
	$y = 0.0024 \cdot x + 0.434$	0.9399	0.020	100 – 2000

 $<sup>^*</sup>$  x – is given in  $\mu$ M, y – in  $\mu$ A; sensitivity was evaluated in the defined LDR.

# 3.2. Electroanalytical performance of electrodes modified with electrodeposited Cu-NPs and Ni-NPs in the electrooxidation reaction of UA

Although the linear dynamic ranges (LDRs) and limits of quantification (LOQ) for UA were similar for both electrodes (1.6  $\mu$ M for Cu-NPs and 1.7  $\mu$ M for Ni-NPs), consistent with previous reports (see **ESI**, **Table S1** [41–48]), an unexpected trend was observed. Despite their higher surface roughness (**ESI**, **Fig. S3**) and enhanced ECSA, the Ni-NPs-modified electrodes showed lower sensitivity toward UA electrooxidation across all tested concentrations (Table 2). In contrast, electrodes modified with electrodeposited Cu-NPs, despite having significantly lower roughness and ESCA (0.021 $\pm$ 0.003 cm² vs. 0.12  $\pm$ 0.03 cm² found for Ni-NPs), demonstrated superior sensitivity toward UA under alkaline conditions, Table 2.

The characteristic shape of the CV plots recorded from both electrodes during the electrooxidation of UA was very similar, with an onset potential at 0.1 V, Fig. 2A. However, differential currents of the second cycle of CV revealed that the concentration of oxygen involved in the electroreduction reaction in the cathodic range was lower for Cu-NPs compared to the background solution, ESI, Fig. S5. This suggests a difference in interaction with oxygen on Cu-NPs compared with Ni-NPs (see Section 3.4).

It is important to note that the improved sensitivity of Cu-NPs-modified electrodes is primary responsible for the increased current/signal intensity in UA electrooxidation, but this does not necessarily correlate with analyte specificity. Therefore, specificity tests were conducted using both types of electrodes. Surprisingly, the electrode modified with electrodeposited Cu-NPs exhibited a poorer response in the specificity test conducted in AM mode compared to the Ni-NPs-based electrode, Fig. 2B

Thus, in addition to the response recorded for UA at an applied potential of 0.2 V, signals corresponding to the electrooxidation of EtOH, ethanol amine, urea and ascorbic acid were also detected, Fig. 2B, line a. In other words, in real samples, an additive electrochemical response towards multiple electroactive species can be expected from the electrode modified with electrodeposited Cu-NPs.

In contrast, the electrode based on electrodeposited Ni-NPs, which initially exhibited low sensitivity in the electrooxidation reaction with UA (Table 2), showed exclusive specificity for UA, Fig. 2B, *line b*. This phenomenon is hypothesized to stem from differences in the interactions among UA, molecular oxygen, and the defect oxides present on the surfaces of Cu-NPs and Ni-NPs (*see Section 3.4*).

#### 3.3. First-principles calculations

In search of the answer to the improved specificity of Ni-NPs-based electrodes compared to Cu-NPs analogues in UA electrooxidation reactions, the polarizabilities of the monovalent (U1) and divalent (U2) anions of UA and their complexes with copper and nickel cations/atoms

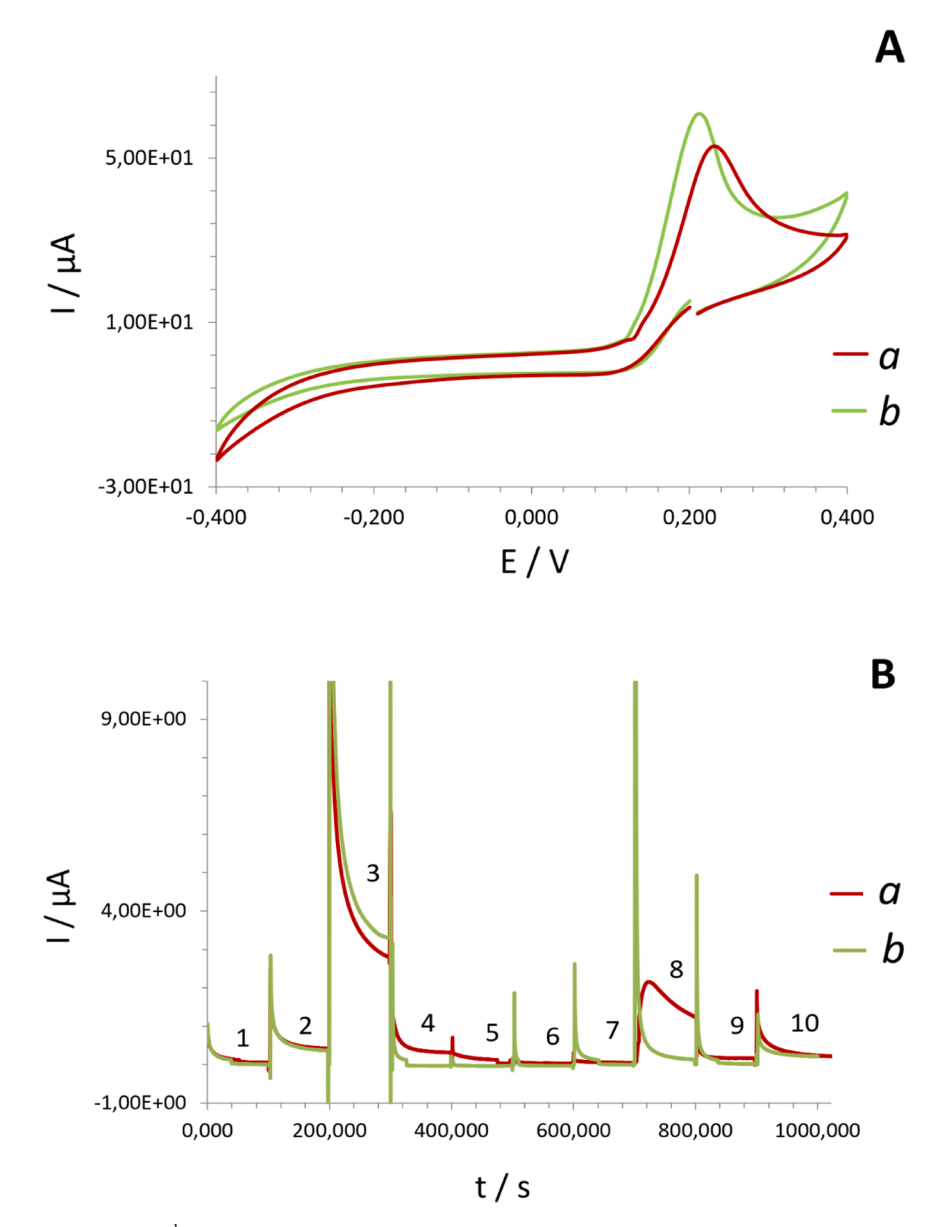


Fig. 2. (A) CV plots recorded at 50 mV/s ( $2^{nd}$  scans shown) at ambient conditions from the electrodes modified with Cu-NPs (a) and Ni-NPs (b). (B) – AM curves indicating the specificity of tested electrodes: 1 – buffer; 2 – 100  $\mu$ M UA; 3 – 1 mM UA, 4 – buffer; 5 – 10 mM EtOH; 6 – 10 mM glycerol; 7 – 10 mM ethylamine; 8 – 10 mM ethanol amine; 9 – 1 mM urea; 10 – 100  $\mu$ M of ascorbic acid. *Note*: pH of all test solutions was  $9 \pm 0.2$ .

(Cu $^+$ , Cu $^{2+}$ , Ni $^{2+}$ , Ni $^{3+}$ ) were calculated using quantum chemistry methods. The magnitude of polarizability characterizes the mobility of the electron cloud in UA. In brief, a higher polarizability enhances the system's ability to transfer charge, *i.e.*, its tendency to undergo oxidation.

The optimized structures of mono- and di-charged anions of UA (U1 and U2) and their corresponding complexes U1M and U2M (where M= Cu,  $\text{Cu}^+,\ \text{Cu}^{2+},\ \text{Ni},\ \text{Ni}^{2+},\ \text{Ni}^{3+})$  with lowest energy configurations are summarized on Fig. 3. The corresponding calculated polarizabilities are summarized in Table S2, ESI.

It is evident that the formation of complexes between the mono- and di-anions and metal atoms/ions (Cu, Cu $^+$ , Cu $^{2+}$ , Ni, Ni $^{2+}$ , Ni $^{3+}$ ) results in an increase in the system's polarizability, *i.e.*, enhanced mobility of the electron cloud, which, in turn, facilitates the subsequent oxidation of U1 and U2. Briefly, for both anions (U1 and U2), polarizability increases upon complexation with metal species in the following order (ESI, Table S2):

$$\begin{array}{l} U1 < U1Cu^{+} < U1Cu^{2+} < U1Ni^{3+} < U1Ni^{2+} < U1Cu < U1Ni \\ U2 < U2Cu^{+} < U2Cu^{2+} < U2Ni^{3+} < U2Ni^{2+} < U2Cu < U2Ni \\ \end{array}$$

The polarizability of complexes formed between the mono- and dicharged UA anions (U1, U2) and nickel atoms or ions is higher than that of the free U1 and U2 species. In other words, the mobility of the electron cloud in these complexes is greater than in the free U1 and U2 systems or analogues with copper.

This result could explain the enhanced specificity of electrodes modified with Ni-NPs towards UA (Fig. 2B, line b). However, based on the calculations, enhanced specificity should be expected for the complexes formed between the neutral metal atoms and UA, viz. U1Cu, U1Ni, U2Cu, U2Ni. In other words, specificity should increase as defect oxides decrease. Yet, our previous study showed that the specificity of target analyte detection increases with the increase of defect oxides [17].

This discrepancy suggests that, in addition to polarizability, the specificity of UA detection on the surface of electrodeposited NPs may also be influenced by oxygen, either as part of defect oxides or as molecular oxygen present in the droplet.

In the next step, the change in total charge of the mono- and dicharged anions of UA (U1, U2) upon the attachment of molecular

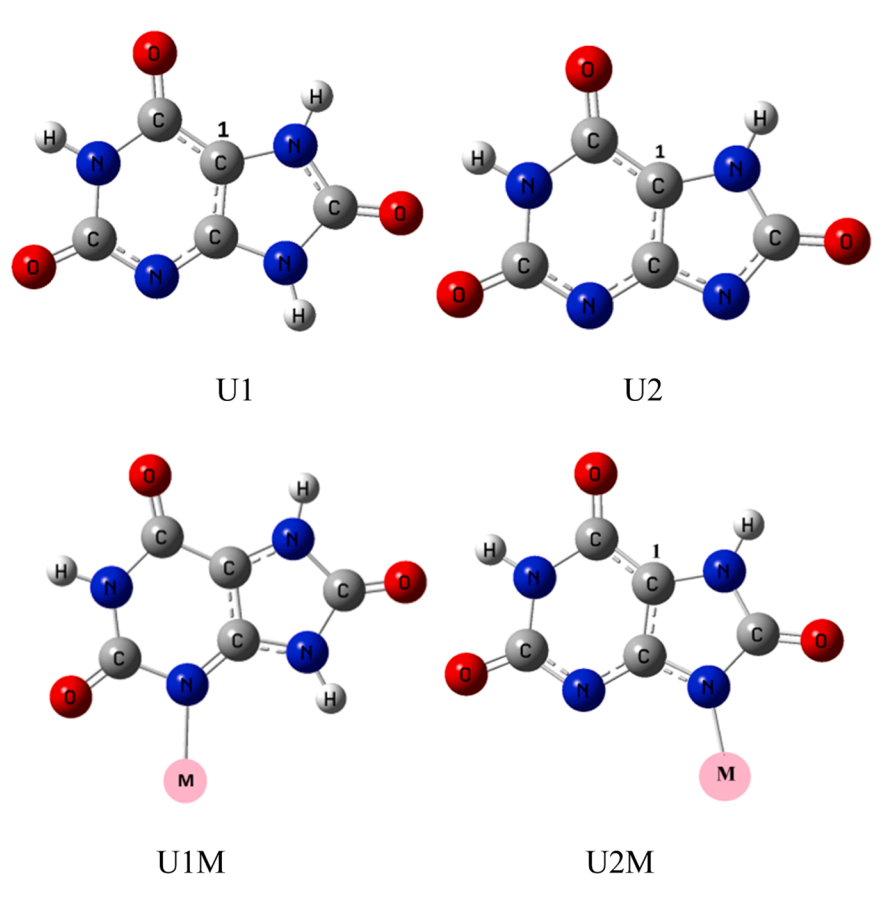


Fig. 3. The optimized structures of one-charged (U1) and two charged (U2) anions of UA and schematic illustration of their complexes U1M and U2M with atoms and ions of metals  $(M = Cu, Cu^+, Cu^{2+}, Ni, Ni^{2+}, Ni)^{3+}$ .

oxygen and metal atoms (ions) to U1 and U2 was calculated, **Table S3**. This change characterizes the transfer of electronic density from the mono- and di-charged anions of UA during the formation of the U1O<sub>2</sub>, U2O<sub>2</sub> and U1O<sub>2</sub>M, and U2O<sub>2</sub>M complexes, Fig. 4.

Remarkably, that charge transfer from UA during the attachment of  $O_2$  and M (M=Cu,  $Cu^+$ ,  $Cu^{2+}$ , Ni, Ni<sup>2+</sup>, Ni<sup>3+</sup>) was minimal for the neutral atoms (Ni and Cu), that agrees with the results of a previous study [17] (no defect oxides  $\leftrightarrow$  few or no real catalytic centers  $\leftrightarrow$  limited formation of complexes with UA under ambient conditions). Regardless of the UA structure (U1 or U2), the maximal charge transfer during the attachment of molecular oxygen and M (M=Cu,  $Cu^+$ ,  $Cu^{2+}$ , Ni, Ni<sup>2+</sup>, Ni<sup>3+</sup>) occurred for copper ions, particularly  $Cu^{2+}$ , ESI, Table S3. This supports the earlier assumption that an increase in polarizability is not the sole factor enhancing UA oxidation capacity.

The significant difference in values obtained for the catalytic centers of copper (-0.518 found for U1Cu $^{+}\mathrm{O}_{2,}$  -1.228 for U1Cu $^{2}\mathrm{+}\mathrm{O}_{2,}$  -0.698 for U2Cu $^{+}\mathrm{O}_{2}$  and -1.537 for U2Cu $^{2}\mathrm{+}\mathrm{O}_{2}$ ) vs nickel (-1.08 for U1Ni $^{2}\mathrm{+}\mathrm{O}_{2}$  and -0.972 for U2Ni $^{2}\mathrm{+}\mathrm{O}_{2,}$  ESI, Table S3) suggests different interaction mechanisms between UA, molecular oxygen and the surface of electrodeposited Cu-NPs and Ni-NPs, represented by defect oxides (see the next section).

# 3.4. Influence of molecular oxygen in electrooxidation of UA by electrodeposited Cu-NPs and Ni-NPs

It is believed that the oxidation of UA in aqueous solutions begins with the attachment of oxygen [25]. However, in the present study, using oxygen mini-sensor, no significant oxygen consumption was recorded in a droplet of UA at alkaline pH in the absence of electrocatalysts, **ESI**, **Fig. S6**. Thus, no oxygen consumption was observed in a droplet of UA placed on a Petri dich in the absence of polarization that

suggests that extensive chemical oxidation of UA did not occur under the conditions used. On the other hand, this allows us to attribute the observed signal in the anodic range of potentials (Fig. 2A) exclusively to the electrocatalytic oxidation of UA by electrodeposited Cu-NPs and Ni-NPs.

Interestingly, in a droplet of UA placed on the surface of the electrode modified with Ni-NPs and under applied polarization, the oxygen consumption remained at the same level as recorded for an UA droplet placed on the surface of a Petri dish in the absence of electrocatalysts and polarization (ESI, Fig. S5). In other words, no oxygen consumption occurred under applied polarization in a droplet of UA at alkaline pH on the surface of electrodes modified with electrodeposited Ni-NPs; however, electrooxidation did occur, see Fig. 2. Based on this, it can be assumed that the electrodeposited Ni-NPs electrocatalyst does not require an oxygen supply for efficient UA electrooxidation at alkaline pH.

In contrast, significantly greater oxygen consumption was recorded under the applied polarization in a droplet of UA placed on the surface of the electrode modified with Cu-NPs. This observation suggests that: (*i*) molecular oxygen is more likely involved in the oxidation of UA on the surface of Cu-NPs; and (*ii*) the mechanism of UA electrooxidation on the Ni-NPs-based electrode differs from that on the Cu-NPs-based electrode under applied polarization.

Moreover, intensive oxygen consumption at alkaline pH was detected on the surface of Cu-NPs even in the absence of UA (Fig. 5A, dashed line). At the same time, the gradual increase in oxygen consumption in the analyzed droplet of UA on Cu-NPs was less pronounced compared with the background solution applied at the same pH, Fig. 5A, solid line. The obtained data allows us to conclude that, in the presence of UA, at least two concurrent reactions (interaction of Cu-NPs with oxygen and UA electrooxidation by Cu-NPs) are taking place simultaneously.

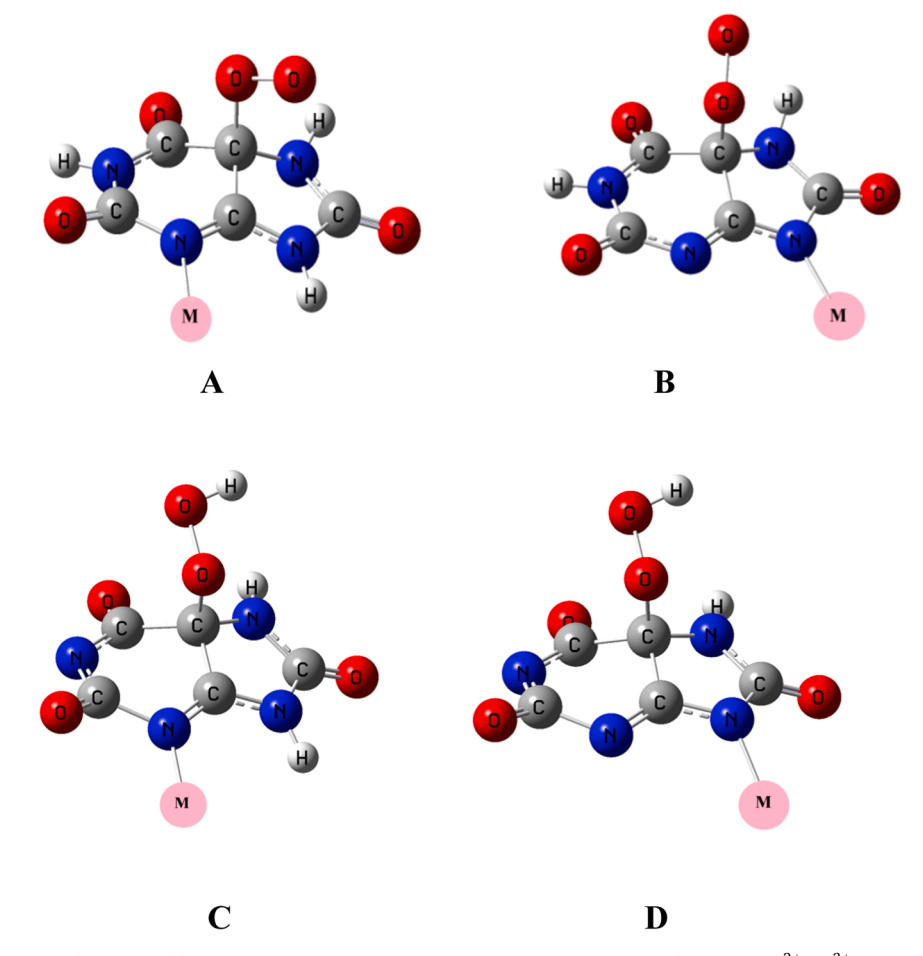


Fig. 4. Schematic representation of energetically advantageous structures: (A) U1MO<sub>2</sub> and (B) U2MO<sub>2</sub>, where  $M = Cu^{2+}$ , Ni<sup>3+</sup>, (C) U1MO<sub>2</sub>, M = Cu, Cu<sup>+</sup>, Ni, Ni<sup>2+</sup>, (D) U2MO<sub>2</sub>,  $M = Ni^{3+}$ , Ni<sup>2+</sup>, Ni, Cu<sup>+</sup>, Cu. *Note*: for the cases (C) and (D), there is a transfer of a hydrogen atom from the six-membered ring to the attached O<sub>2</sub> molecule, resulting in the formation of a peroxide group.

In contrast, no oxygen consumption was observed at alkaline pH on the surface of electrodeposited Ni-NPs (Fig. 5B, dashed line). Only a small amount of oxygen consumption, at approximately  $\sim 25~\mu$ mol/L (calculated as the difference between the baseline of the oxygen mini-sensor and the minimal value obtained during the CV plot for three cycles), was detected during electrooxidation of UA, Fig. 5B, solid line.

Notably, the same level of oxygen consumption was recorded for 2 mM of UA dropped on the surface of a Petri dish (ESI, Fig. S5). This indicates that UA electrooxidation on Ni-NPs modified electrodes occurs with minimal oxygen involvement. This result was in line with the previously reported trend obtained for defect nickel oxides, which, when transferred to an alkaline pH, form [NiO $_{\rm X}$ (OH) $_{\rm y}$ ], leading to a decrease of oxygen adsorption [39,40].

To sum it up, it can be assumed that UA electrooxidation on the surface of Cu-NPs may be affected by oxygen participation, which impacts the results of the specificity test (Fig. 2B).

This assumption was confirmed by subsequent specificity test conducted in AM mode in the absence of molecular oxygen. For this test, all test solutions, including UA and all interfering electroactive species were prepared in oxygen-free OXCAL solution maintaining 0  $\mu$ mol/L of oxygen, **ESI, Fig. S7**. The results of this test are summarized in Fig. 6.

Briefly, Cu-NPs-based electrodes tested in oxygen-free OXCAL solutions, in the absence of oxygen apart from UA, showed much higher response towards interfering species, *e.g.*, amines, ascorbic acid and urea than to UA. However, in the presence of oxygen (see Fig. 2B), the same electrode showed no pronounced response to urea, ascorbic acid, and ethylamine, with signal intensities comparable to or below that of the electrooxidation of 1 mM UA. In other words, changes in oxygen

concentration (from 21 % to 0 %) in a droplet of UA dramatically affected the performance of electrodes modified with electrodeposited Cu-NPs coated with defect oxides (see Table 1).

In contrast, despite the pronounced decrease in sensitivity in the absence of oxygen Ni-NPs based electrodes exhibited exclusive specificity to UA. It is believed to be due to the inertness of Ni-NPs to oxygen under the given conditions. Therefore, the performance, e.g., specificity of Ni-NPs in UA electrooxidation reaction cannot be significantly affected by the presence/or absence of oxygen.

To conclude, this set of experiments demonstrates that electrodeposited Cu-NPs and Ni-NPs exhibit different behaviours towards interaction with oxygen, which result in differences in the UA electrooxidation reaction. At the same time, the mentioned difference may be related to the various composition of electrode surfaces (surface chemistry), *see* Section 3.5.

#### 3.5. Importance of defect oxides on the surface of electrodeposited Cu-NPs and Ni-NPs in the presence of oxygen

Defects-rich Cu-NPs and Ni-NPs, when used as electrocatalysts in electrooxidation of urea and UA metabolites in alkaline solutions, intrinsically possess higher catalytic activity than defect-less NPs [17,49, 50].

Thus, the importance of nickel oxide lattice defects for efficient oxygen evolution reaction has been emphasized in several studies [39,40]. Defect nickel oxides, when transferred to alkaline pH, form [NiO $_{\rm X}(-{\rm OH})_{\rm y}]$ , which significantly alters their behaviour in the oxygen evolution reaction. More importantly, these Ni-NPs do not adsorb oxygen at this

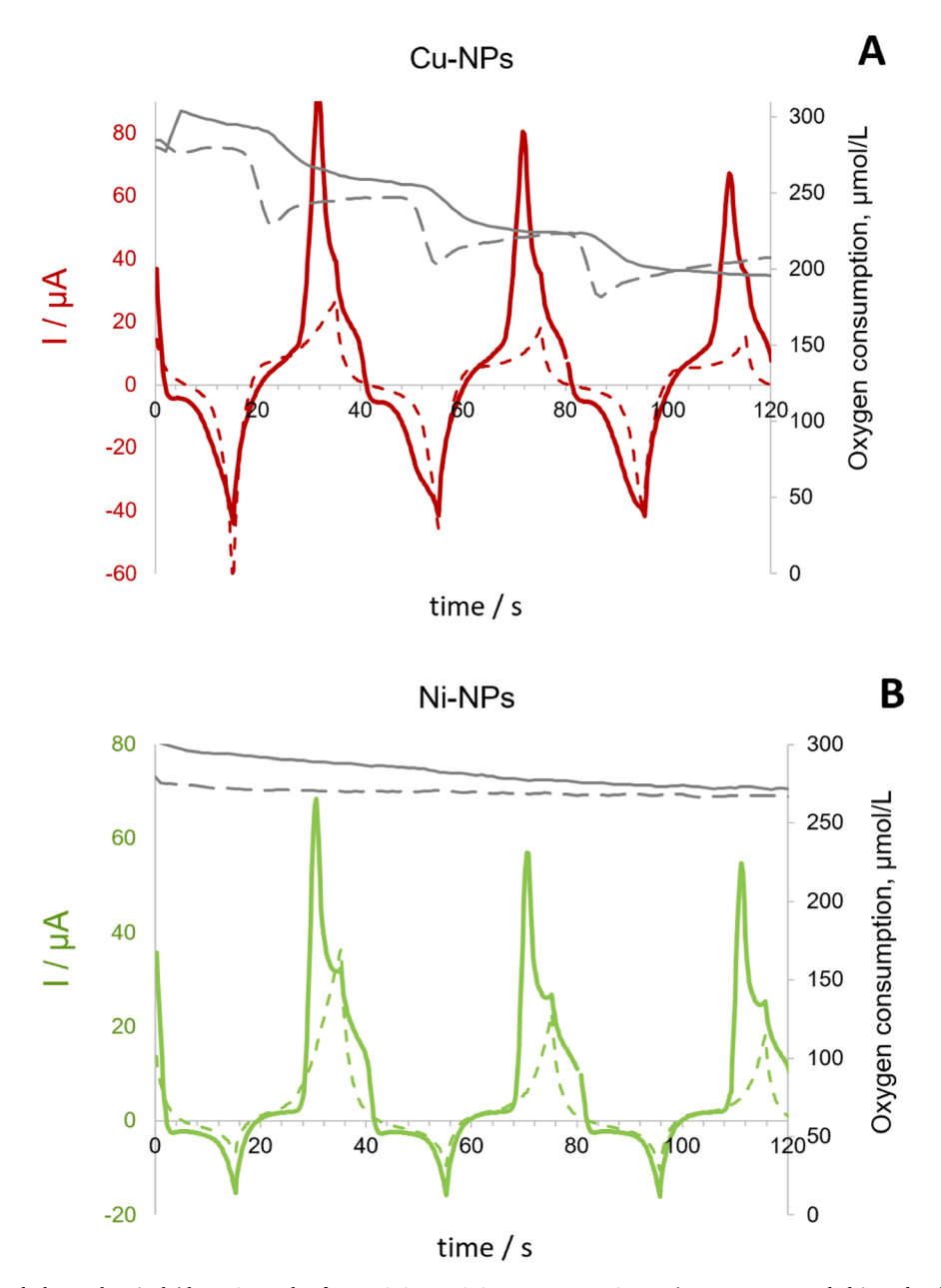


Fig. 5. Overlaid oxygen and electrochemical (three CV cycles from -0.4 V to 0.4 V, scan rate 50 mV/s) responses recorded in a droplet of background solution (dashed line) and 2 mM UA (solid line) from electrodes modified with electrodeposited Cu-NPs (A) and Ni-NPs (B). Note: 2 mM UA was applied to make the observed trends pronounced; pH of solutions was  $9.0 \pm 0.2$ . The basic line of the oxygen mini-sensor at  $20\pm2$  °C is  $280\pm20$  µmol/L. The measurements were performed in triplicate and yielded the same results.

pH [39,40] which is consistent with the results obtained in our study, ESI, Fig. S6 and Fig. 5B.

Therefore, to verify the impact of surface chemistry of electrodeposited NPs on their performance in the presence of molecular oxygen, we next reduced the surface oxides in alkaline solutions containing hydrazine ( $N_2H_4$ ), a known reducing agent for copper and nickel oxides [51–53]. Treatment with  $N_2H_4$  removes lattice oxygen, resulting in changes to the oxygen vacancies in oxides [54]. In other words, this approach enables changes in the surface chemistry of electrodeposited NPs.

For this end, a droplet of 100 mM  $N_2H_4$ , prepared in a background solution with pH  $9.0\pm0.2$  was placed on the electrodes modified with electrodeposited Cu-NPs and Ni-NPs, following by cycling in CV at 20 mV/s from -0.4 V to 0.05 V for 10 scans. Subsequently, the  $N_2H_4$ -treated electrodes were thoroughly rinsed with DI-water and re-tested in both the background solution and in the presence of 2 mM UA.

The change in surface chemistry of electrodes after  $N_2H_4$  treatment was confirmed via subsequent CV studies. Briefly, the peak maximum corresponding to the electrooxidation UA at alkaline pH for the electrode modified with Cu-NPs was shifted to the anodic range by approximately  $\sim\!0.15$  V, and by approximately  $\sim\!0.2$  V for the Ni-NPs-based electrodes, **ESI, Fig. S8**. Moreover, the shape of the CV plots was significantly altered, indicating that the surface chemistry of the electrodes had been successfully modified (*see in comparison with* Fig. 2A).

The oxygen consumption plot recorded from the surface of  $N_2H_4$ -treated electrodes in alkaline background electrolyte and UA solutions containing oxygen, under applied polarization revealed an opposite trend compared to what was observed in Section 3.4. Specifically, Cu-NPs modified electrodes with reduced surface oxides (most probably reduced  $Cu_2O$ ) no longer absorb oxygen anymore (Fig. 7A), in contrast to intact electrodes (Fig. 5A). In general, the oxygen consumption profile

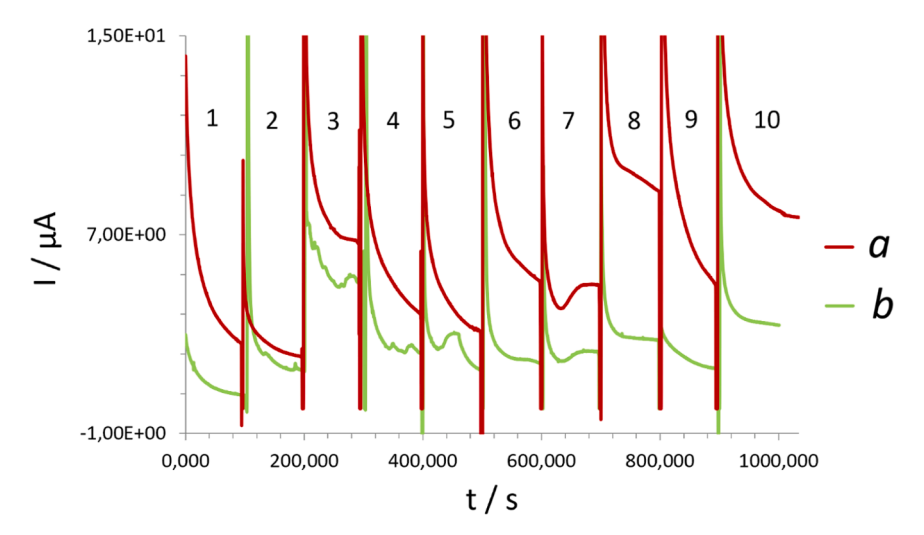
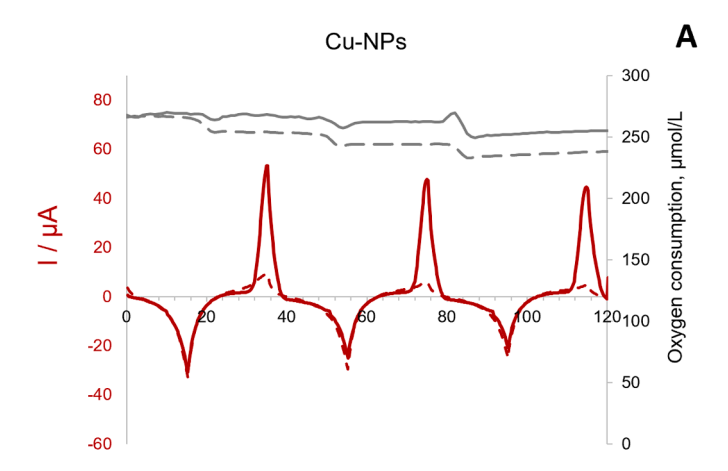
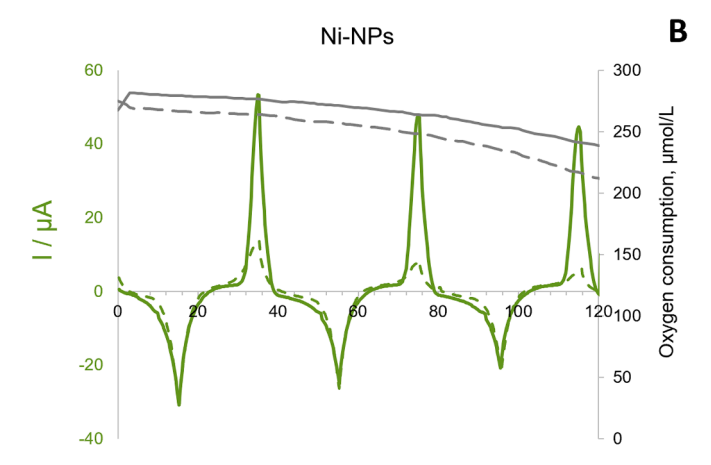


Fig. 6. AM curves indicating the specificity of the tested electrodes modified with Cu-NPs (a) and Ni-NPs (b) in the absence of oxygen: 1- oxygen-free OXCAL solution;  $2-100~\mu$ M UA; 3-1~mM UA, 4- oxygen-free OXCAL solution; 5-10~mM EtOH; 6-10~mM glycerol; 7-10~mM ethylamine; 8-10~mM ethanol amine; 9-1~mM urea;  $10-100~\mu$ M of ascorbic acid. Note: all solutions with pH  $9.0~\pm~0.2$  were prepared in oxygen-free OXCAL solution. The measurements were performed in triplicate and yielded the same results.





**Fig. 7.** Overlaid oxygen and electrochemical responses (three CV cycles from -0.4 V to 0.4 V, scan rate 50 mV/s) recorded simultaneously in a droplet of background electrolyte (*dashed line*) and 2 mM UA (*solid line*) from electrodes modified with electrodeposited Cu-NPs (**A**) and Ni-NPs (**B**) after reduction of their surface. *Note*: 2 mM UA was applied to make the observed trends pronounced; pH of solutions was  $9.0 \pm 0.2$ . The basic line of the oxygen minisensor at  $20\pm2$  °C is  $280\pm20$  umol/L.

of Cu-NPs with a modified surface chemistry closely resembled the profile recorded for the intact Ni-NPs (Fig. 5B).

In contrast, the electrodes modified with electrodeposited Ni-NPs, after their surface chemistry was modified with hydrazine, surprisingly began to absorb molecular oxygen in alkaline solutions, Fig. 7B

Notably, the oxygen consumption in the background solution was more pronounced (*dashed line*) compared to that in the solution containing UA at the same alkaline pH (*solid line*). A similar trend was observed for the intact electrodes modified with Cu-NPs (see Fig. 5A). It is hypothesized that the reduction of surface of Ni-NPs in hydrazine solution affected the ratio between defect Ni<sup>3+</sup>, nickel oxides and hydroxides (Table 1).

In Section 3.4, the role of molecular oxygen in the specificity of electrochemical oxidation of UA in alkaline solutions by electrodes based on electrodeposited NPs was examined. It was shown that in the absence of oxygen Cu-NPs lost their specificity in UA electrooxidation reactions (Fig. 6). In contrast, Ni-NPs analogues were able to maintain the excellent specificity toward UA because their catalytic activity was independent on oxygen adsorption/presence of oxygen. In the present experiment, the role of surface chemistry of electrodeposited NPs on the adsorption of molecular oxygen was emphasized. The difference in oxygen adsorption on the surface of  $N_2H_4$ -treated Cu-NPs and Ni-NPs, compared with their intact surfaces, indicates that oxygen adsorption is a function of the surface chemistry of electrodeposited NPs.

In this regard, in can be concluded that both the presence of defect oxides on the surface of electrodeposited NPs and the presence of molecular oxygen in a droplet of the test solution, along with its interaction with NPs, determine the specificity of UA electrooxidation at alkaline pH.

# 3.6. Toward mechanistic aspects of UA electrooxidation using electrodeposited Cu-NPs and Ni-NPs

A deeper understanding of the reaction mechanisms and the role of interfacial interactions is essential for designing more specific electrocatalysts. Based on the results summarized above, it can be hypothesized that the electrooxidation of UA on the surface of electrodeposited NPs occurs in several steps: (1) adsorption of UA; (2) polarization of one and di-charged anions of UA; (3) interaction of polarized ions with the defect oxides of NPs; (4) reduction of the defect oxides of NPs in the presence of UA; (5) oxidation of the reduced species in the oxides under the applied polarization; (6) signal read-out in the anodic range of potentials.

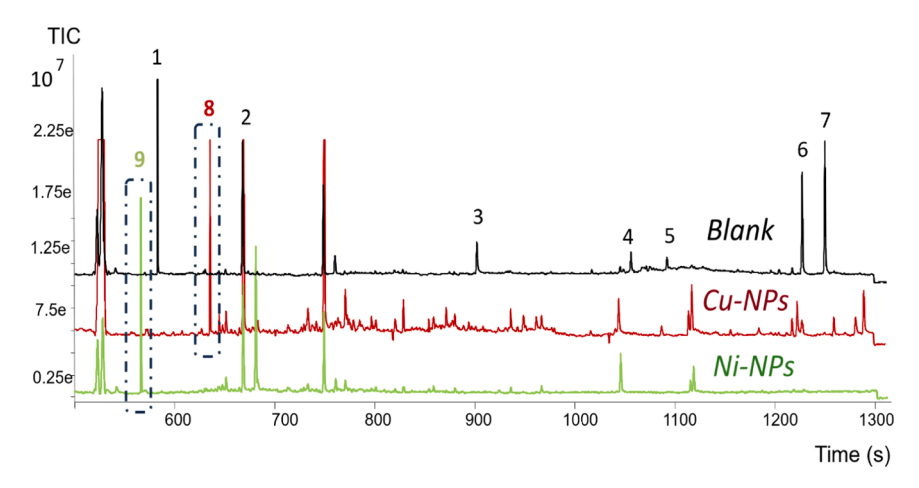


**Fig. 8.** GC–MS chromatograms obtained for the UA droplets collected after microelectrolysis and derivatized with MSTFA: 1 – diethyl azodicarboxylate; 2 – 5,6-dihydro-3-methyl-1-(trimethylsilyl)oxymethyl uracil; 3 – N'-cyclooctyl-N,N-dimethyl urae; 4 – 1-lodo-2-methylundecane; 5 – 1-methyl anthracene; 6 – 2-tert-butyl-6-methylphenol, trimethylsilyl ether; 7 – 2,2'-methylenebis[6-(1,1-dimethylethyl)-4-methyl phenol; 8 – 2,5-dihydro-2,5-dioxo- 3-furanacetic acid; 9 – 1,2,5-oxadiazole. *Note*: unmarked peaks are attributed to thermo degraded MSTFA products due to the pre-treatment procedure (see *Experiment*).

Importantly, step (1) on the surface of Cu-NPs can be significantly affected by altered interaction with oxygen at alkaline pH (see Section 3.3), leading to a loss of specificity towards UA. In contrast, Ni-NPs do not adsorb oxygen under the same experimental conditions, which prevents interference with UA adsorption. This suggests that the subsequent steps (2) - (5) on Ni-NPs may follow different pathways compared to those occurring on the surface of Cu-NPs.

This assumption was confirmed by subsequent GC–MS studies of the droplets collected after electrooxidation UA (see Experiment). The GC-profile of the chromatogram obtained for the droplet collected after microelectrolysis on the Cu-NPs modified electrode differed from that of the sample obtained from the Ni-NPs based electrode, Fig. 8. In general, the total number of intermediate compounds formed on the Cu-NPs-based electrode was much higher ( $\geq$ 515) compared to the spectrum of compounds ( $\geq$ 256) obtained after electrooxidation on the Ni-NPs-modified electrode. This observation indirectly suggests a more complete electrochemical conversion of UA into products on Ni-NPs.

Moreover, *peak/compound 3* (Fig. 8, see chromatogram corresponding to the blank sample), which is related to an urea derivative and formed as a thermal degradation product of free 2 mM UA (see *Experiment*, derivatization protocol with MSTFA), was still detected in the sample subjected to microelectrolysis on Cu-NPs (Fig. 8, see chromatogram corresponding to Cu-NPs). This suggests that UA remains partly unreacted/non-oxidized after microelectrolysis on Cu-NPs. In contrast, *peaks/compounds 1, 3, 4, 5, 6,* and 7 were not detected in samples after electrooxidation on Ni-NPs, highlighting a different electrooxidation pathway for UA on Ni-NPs.

Notably, the main characteristic peaks, detected with pronounced signal intensities, allowed us to distinguish the electrooxidation pathways of UA on Cu-NPs vs. Ni-NPs. These peaks were attributed to the formation of 2,5-dihydro-2,5-dioxo-3-furanacetic acid (peak 8) and 1,2,5-oxadiazole (peak 9), respectively.

To sum it up, the interaction between UA and electrodeposited Ni electrocatalyst follows a different pathway than that occurring on Cu-NPs. Importantly, the reaction intermediates play a key role in controlling the electrochemical reaction route and the specificity of UA electrooxidation. However, these intermediates may not be the primary steps in the overall pathway. The difference in the formation of electrooxidation intermediates of UA may stem from the distinct nature of oxygenic species participated in reaction on Ni-NPs and Cu-NPs surface (see Sections 3.4, 3.5).

#### 4. Conclusions

This study compares the electroanalytical performance of electrodes modified with electrodeposited Cu-NPs and Ni-NPs in the electrooxidation reaction with UA at alkaline pH.

The specificity of electrodes toward UA correlates with the polarizability of mono- and di-anion of UA on the catalytic centers of electrodeposited NPs and the nature of the interaction between the NPs surfaces and molecular oxygen. Thus, the electrodes modified with electrodeposited Ni-NPs, which remain inert to oxygen adsorption and support advanced polarizability of UA compared with Cu-NPs analogues, demonstrated improved performance in specificity tests with UA. Significantly, different interaction with molecular oxygen by electrodes tend to depend on initial surface composition (surface chemistry) of electrodeposited Cu-NPs and Ni-NPs.

Moreover, the different interaction between oxygen and the surface of electrodeposited Ni-NPs and Cu-NPs affected the type of reaction products formed during electrooxidation of UA. The obtained data suggest that the mechanism underlaying the electrooxidation of UA on electrodes modified with electrodeposited Cu-NPs differs from those on electrodes modified with Ni-NPs. However, this question requires further detailed investigations, which are planned for future studies in our laboratory.

### CRediT authorship contribution statement

**E.V. Butyrskaya:** Writing – review & editing, Visualization, Validation, Methodology, Investigation. **N. Korkmaz:** Visualization, Methodology, Investigation, Formal analysis. **E.V. Zolotukhina:** Visualization, Validation, Methodology, Investigation. **S.A. Kleinikova:** Investigation, Formal analysis. **M. Koch:** Methodology, Investigation, Formal analysis. **Y.E. Silina:** Writing – original draft, Validation, Supervision, Funding acquisition, Data curation, Conceptualization.

### **Declaration of competing interest**

The authors declare that they have no known competing financial interests or personal relationships that could have appeared to influence the work reported in this paper.

#### Acknowledgements

This study was a part of the research program of Y.E.S. funded by the Deutsche Forschungsgemeinschaft (DFG, German Research Foundation,

project 427949628).

The authors thank Dr. P. Herbeck-Engel (INM – Leibniz Institute for New Materials, Saarbrücken, Germany) for the RAMAN measurements.

The work of E.V.Z. and S.A.K. was supported within the thematic map 124013000692-4.

#### Supplementary materials

Supplementary material associated with this article can be found, in the online version, at doi:10.1016/j.electacta.2025.147012.

#### Data availability

Data will be made available on request.

#### References

- M. Bernal Lopez, J. Ustarroz, Electrodeposition of nanostructured catalysts for electrochemical energy conversion: current trends and innovative strategies, Curr. Opin. Electrochem. 27 (2021) 100688, https://doi.org/10.1016/j. coelec.2021.100688.
- [2] M. Miao, H. Duan, J. Luo, X. Wang, Recent progress and prospect of electrodeposition-type catalysts in carbon dioxide reduction utilizations, Mater. Adv. 3 (2022) 6968–6987, https://doi.org/10.1039/d2ma00775d.
- [3] I. El-Hallag, S. Elsharkawy, S. Hammad, The effect of electrodeposition potential on catalytic properties of Ni nanoparticles for hydrogen evolution reaction (HER) in alkaline media, J. Appl. Electrochem. 52 (2022) 907–918, https://doi.org/ 10.1007/510800-022-01679-w
- [4] Y.E. Silina, One-step electrodeposited hybrid nanofilms in amperometric biosensor development, Anal. Methods 16 (2024) 2424–2443, https://doi.org/10.1039/ D4AY00290C
- [5] E.V. Zolotukhina, E.V. Butyrskaya, M. Koch, P. Herbeck-Engel, M.G. Levchenko, Y. E. Silina, First principles of hydrazine electrooxidation at oxide-free and oxide-based palladium electrodes in complex media, Phys. Chem. Chem. Phys. (2023), https://doi.org/10.1039/D3CP00829K.
- [6] Y.E. Silina, F. Meier, V.A. Nebolsin, M. Koch, D.A. Volmer, Novel galvanic nanostructures of Ag and Pd for efficient laser desorption/ionization of low molecular weight compounds, J. Am. Soc. Mass Spectrom. 25 (2014) 841–851, https://doi.org/10.1007/s13361-014-0853-8.
- [7] L. Zhao, Y. Guo, C. Fu, L. Luo, G. Wei, S. Shen, J. Zhang, Electrodeposited PtNi nanoparticles towards oxygen reduction reaction: a study on nucleation and growth mechanism, Chin. J. Catal. 42 (2021) 2068–2077, https://doi.org/10.1016/51872-2067(21)63860-3.
- [8] Y. Zhang, L. Liu, C. Sun, Y. Du, Y. Zhou, Q. Xie, NaBH4-electrooxidation mediated electrodeposition of catalytic Pt nanoparticles on a honeycomb-gold electrode for hydrogen evolution reaction, J. Alloys Compd. 888 (2021) 161564, https://doi. org/10.1016/j.jallcom.2021.161564.
- [9] S. Li, X. Yan, M. Shi, P. Wei, H. Lu, Z. Zhang, Y. Zhang, Y. Li, Electrodeposition of Pt-Ni nanoparticles on graphene as an electrocatalyst for oxygen reduction reaction, Front. Chem. 10 (2022) 1–8, https://doi.org/10.3389/ fchem.2022.1061838.
- [10] A. Góral, Nanoscale structural defects in electrodeposited Ni/Al2O3 composite coatings, Surf. Coat. Technol. 319 (2017) 23–32, https://doi.org/10.1016/j. surfroat 2017 03 061
- [11] Y. Jia, K. Jiang, H. Wang, X. Yao, The role of defect sites in nanomaterials for electrocatalytic energy conversion, Chem 5 (2019) 1371–1397, https://doi.org/ 10.1016/j.chempr.2019.02.008.
- [12] Q. He, L. Han, C. Lin, K. Tao, A review on defect modulated electrocatalysts for the oxygen evolution reaction, Nanoscale 16 (2024) 12368–12379, https://doi.org/ 10.1039/d4nr01805b.
- [13] M. Serhan, M. Sprowls, D. Jackemeyer, M. Long, I.D. Perez, W. Maret, N. Tao, E. Forzani, Total iron measurement in human serum with a smartphone, in: AIChE Annu Meet Conf Proc 2019-Novem, 2019, https://doi.org/10.1039/x0xx000000x.
- [14] Z. Guo, M. Bi, H. He, Z. Liu, Y. Duan, W. Cao, Defect engineering associated with cationic vacancies for promoting electrocatalytic water splitting in iron-doped Ni2P nanosheet arrays, J. Colloid Interface Sci. 654 (2024) 785–794, https://doi. org/10.1016/j.jcis.2023.10.047.
- [15] F. Fasulo, A. Massaro, A. Pecoraro, A.B. Muñoz-García, M. Pavone, Role of defect-driven surface reconstructions in transition metal oxide electrocatalysis towards OER/ORR: a quantum-mechanical perspective, Curr. Opin. Electrochem. 42 (2023) 101412, https://doi.org/10.1016/j.coelec.2023.101412.
- [16] Y. Zhu, Y. Zhao, C. Xi, K. Hu, S. Han, J. Jiang, Cationic defect engineering induces LOM-enhanced electrocatalysts derived from in situ semi-transformed NiFe-LDH/ MOF heterostructure for efficient overall water-splitting, Compos. B Eng. 298 (2025) 112356. https://doi.org/10.1016/j.compositesb.2025.112356.
- [17] E.V. Butyrskaya, E.V. Zolotukhina, P. Herbeck-Engel, M. Koch, Y.E. Silina, Toward the development of a specific non-enzymatic amperometric sensor for determining uric acid in fermentation samples, Microchim. Acta 192 (2025), https://doi.org/ 10.1007/s00604-025-06979-4.
- [18] S. Verma, A. Sen, N. Dutta, P. Sengupta, P. Chakraborty, G. Dutta, Highly specific non-enzymatic electrochemical sensor for the detection of uric acid using

- carboxylated multiwalled carbon nanotubes intertwined with GdS-Gd2O3 nanoplates in Human urine and serum, Langmuir 40 (2024) 21427–21441, https://doi.org/10.1021/acs.langmuir.4c02233.
- [19] A.K. Gunasekaran, N. Nesakumar, B.M. Gunasekaran, A.J. Kulandaisamy, J. B. Balaguru Rayappan, Highly sensitive non-enzymatic electrochemical sensor for uric acid detection using copper oxide nanopebbles-modified glassy carbon electrode, Appl. Surf. Sci. 697 (2025) 162956, https://doi.org/10.1016/j.apsusc.2025.162956.
- [20] V. Nagal, T. Tuba, V. Kumar, S. Alam, A. Ahmad, M.B. Alshammari, A.K. Hafiz, R. Ahmad, A non-enzymatic electrochemical sensor composed of nano-berry shaped cobalt oxide nanostructures on a glassy carbon electrode for uric acid detection, New J. Chem. 46 (2022) 12333–12341, https://doi.org/10.1039/ d2nj01961b.
- [21] M. Koch, Y.E. Silina, Uric acid detection by hydrogen peroxide independent biosensors: novel insights and applications, Microchem. J. 207 (2024) 112091, https://doi.org/10.1016/j.microc.2024.112091.
- [22] S.D. Giri, A. Sarkar, Estimating surface area of copper powder: a comparison between electrochemical, microscopy and laser diffraction methods, Adv. Powder Technol. 29 (2018) 3520–3526, https://doi.org/10.1016/j.apt.2018.09.034.
- [23] E. Cossar, M.S.E. Houache, Z. Zhang, E.A. Baranova, Comparison of electrochemical active surface area methods for various nickel nanostructures, J. Electroanal. Chem. 870 (2020) 114246, https://doi.org/10.1016/j. jelechem.2020.114246.
- [24] C.L. Benn, P. Dua, R. Gurrell, P. Loudon, A. Pike, R. Ian Storer, C. Vangjeli, Physiology of hyperuricemia and urate-lowering treatments, Front. Med. 5 (2018) 1–28, https://doi.org/10.3389/fmed.2018.00160.
- [25] Horinouchi R., Yamamoto Y., Fujisawa A. (2021) Increase of oxidation rate of uric acid by singlet oxygen at higher pH. 69:16–19. doi:10.3164/jcbn.20.
- [26] R. Horinouchi, Y. Yamamoto, A. Fujisawa, Increase of oxidation rate of uric acid by singlet oxygen at higher pH, J. Clin. Biochem. Nutr. 69 (2021) 16–19, https://doi. org/10.3164/JCBN.20-101.
- [27] L. Debbichi, M.C. Marco de Lucas, J.F. Pierson, P. Krüger, Vibrational properties of CuO and Cu4O3 from first-principles calculations, and raman and infrared spectroscopy, J. Phys. Chem. C 116 (2012) 10232–10237, https://doi.org/ 10.1021/jp303096m.
- [28] D. López-Díaz, J.A. Delgado-Notario, V. Clericò, E. Diez, M.D. Merchán, M. M. Velázquez, Towards understanding the Raman spectrum of graphene oxide: the effect of the chemical composition, Coatings 10 (2020).
- [29] Y. Deng, A.D. Handoko, Y. Du, S. Xi, B.S. Yeo, In situ raman spectroscopy of copper and copper oxide surfaces during electrochemical oxygen evolution reaction: identification of CuIII oxides as catalytically active species, ACS Catal. 6 (2016) 2473–2481, https://doi.org/10.1021/acscatal.6b00205.
- [30] V.S. Levitskii, V.I. Shapovalov, A.E. Komlev, A.V. Zav'yalov, V.V. Vit'ko, A. A. Komlev, E.S. Shutova, Raman spectroscopy of copper oxide films deposited by reactive magnetron sputtering, Tech. Phys. Lett. 41 (2015) 1094–1096, https://doi.org/10.1134/S106378501511022X.
- [31] R. Schennach, A. Gupper, Copper oxidation studied by *In situ* raman spectroscopy, MRS Online Proc. Libr. 766 (2003) 32, https://doi.org/10.1557/PROC-766-E3.2.
- [32] H. Ramachandran, M.M. Jahanara, N.M. Nair, P. Swaminathan, Metal oxide heterojunctions using a printable nickel oxide ink, RSC Adv. 10 (2020) 3951–3959, https://doi.org/10.1039/c9ra08466e.
- [33] D.S. Hall, D.J. Lockwood, S. Poirier, C. Bock, B.R. MacDougall, Raman and infrared spectroscopy of  $\alpha$  and  $\beta$  phases of thin nickel hydroxide films electrochemically formed on nickel, J. Phys. Chem. A 116 (2012) 6771–6784, https://doi.org/10.1021/jp303546r.
- [34] B.S. Yeo, A.T. Bell, *In situ* raman study of nickel oxide and gold-supported nickel oxide catalysts for the electrochemical evolution of oxygen, J. Phys. Chem. C 116 (2012) 8394–8400, https://doi.org/10.1021/jp3007415.
- [35] R. Thundiyil, P. Poornesh, K. Ozga, J. Jedryka, An insight in to microwave induced defects and its impact on nonlinear process in NiO nanostructures under femtosecond and continuous wave laser excitation, RSC Adv. 14 (2024) 30011–30036. https://doi.org/10.1039/D4RA06056C.
- [36] D. Wang, S. Xu, L. Wu, Z. Li, P. Zhu, D. Wang, Spin-phonon coupling in NiO nanoparticle, J. Appl. Phys. 128 (2020), https://doi.org/10.1063/5.0022668.
- [37] A. Adiba, P.N. Meitei, T. Ahmad, Laser-induced modulation of Magnon and Phonon excitations: size and defect dependency in antiferromagnetic NiO nanoparticles with rhombohedral distortion, Next Nanotechnol. 7 (2025) 100098, https://doi. org/10.1016/j.nxnano.2024.100098.
- [38] C. Guillén, J. Herrero, Structural changes induced by heating in sputtered NiO and Cr2O3 thin films as p-type transparent conductive electrodes, Electron. Mater. 2 (2021) 49–59, https://doi.org/10.3390/electronicmat2020005.
- [39] C. Alex, G. Shukla, N.S. John, Introduction of surface defects in NiO with effective removal of adsorbed catalyst poisons for improved electrochemical urea oxidation, Electrochim. Acta 385 (2021) 138425, https://doi.org/10.1016/j. electacta.2021.138425.
- [40] H. Radinger, P. Connor, S. Tengeler, R.W. Stark, W. Jaegermann, B. Kaiser, Importance of nickel oxide lattice defects for efficient oxygen evolution reaction, Chem. Mater. 33 (2021) 8259–8266, https://doi.org/10.1021/acs. chemmater.1c02406.
- [41] S.B. Mullani, A.K. Tawade, S.N. Tayade, K.K.K. Sharma, S.P. Deshmukh, N. B. Mullani, S.S. Mali, C.K. Hong, B.E.K. Swamy, S.D. Delekar, Synthesis of Ni2+ion doped ZnO-MWCNTs nanocomposites using anin situsol-gel method: an ultra sensitive non-enzymatic uric acid sensing electrode material, RSC Adv. 10 (2020) 36949–36961, https://doi.org/10.1039/d0ra06290a.
- [42] J.F. John, D. Dhinasekaran, S. Subashchandran, On-site detection of uric acid using a portable electrochemical device based on a screen-printed electrode modified

- with nickel ferrite, Mater. Today Chem. 47 (2025), https://doi.org/10.1016/j.
- [43] J.F. John, D. Dhinasekaran, S. Subashchandran, Nickel ferrite modified nickel foam with enriched active sites for the efficient electrochemical sensing of uric acid, Mater. Chem. Phys. 315 (2024) 128996, https://doi.org/10.1016/j. matchemphys.2024.128996.
- [44] K. Amarnath, T. Selvi Gopal, A.C. Josephine Malathi, S. Pandiaraj, M. Alruwaili, A. Alshammari, A.N. Alodhayb, C. Abeykoon, A.N. Grace, V.G. Kumar, Electrochemical detection of dopamine and uric acid with Annealed Metal-Organic Framework/MXene (CuO/C/Ti3C2Tx) nanosheet composites for neurotransmitter sensing, ACS Appl. Nano Mater. 8 (2025) 12661–12675, https://doi.org/10.1021/ acsanm.5c01758.
- [45] A.K. Gunasekaran, N. Nesakumar, B.M. Gunasekaran, A.J. Kulandaisamy, J. B. Balaguru Rayappan, Highly sensitive non-enzymatic electrochemical sensor for uric acid detection using copper oxide nanopebbles-modified glassy carbon electrode, Appl. Surf. Sci. 697 (2025) 162956, https://doi.org/10.1016/j.apsusc.2025.162956.
- [46] V. Nagal, S. Masrat, M. Khan, S. Alam, A. Ahmad, M.B. Alshammari, K.S. Bhat, S. M. Novikov, P. Mishra, A. Khosla, R. Ahmad, Highly sensitive electrochemical non-enzymatic uric acid sensor based on cobalt oxide puffy balls-like nanostructure, Bioseps 13 (2023)
- [47] A. Joshi, G. Slaughter, NiFeCo-modified bucky paper electrodes for sensitive and selective uric acid detection, Microchem. J. 208 (2025) 112348, https://doi.org/ 10.1016/j.microc.2024.112348.
- [48] K. Krishnamoorthy, V. Sudha, S.M. Senthil Kumar, R. Thangamuthu, Simultaneous determination of dopamine and uric acid using copper oxide nano-rice modified

- electrode, J. Alloys Compd. 748 (2018) 338–347, https://doi.org/10.1016/j.jallcom.2018.03.118.
- [49] N.K.T. Nguyen, A.H. Nguyen, V Van Pham, M Van Tran, NT Le Huynh, H. T. Nguyen, H.V. Le, A novel enzymeless electrochemical sensor based on Ni(OH) 2–NiO(OH) nanoelectrocatalyst for sensitive and selective detection of uric acid in PBS simulated body fluid, Mater. Chem. Phys. 327 (2024) 129870, https://doi.org/10.1016/j.matchemphys.2024.129870.
- [50] X. Yan, Zhang W Da, Q.T. Hu, J. Liu, T. Li, Y. Liu, Z.G. Gu, Defects-rich nickel nanoparticles grown on nickel foam as integrated electrodes for electrocatalytic oxidation of urea, Int. J. Hydrog. Energy 44 (2019) 27664–27670, https://doi.org/ 10.1016/j.jihydene.2019.09.004.
- [51] D.M. Littrell, D.H. Bowers, B.J. Tatarchuk, Hydrazine reduction of transition-metal oxides, J. Chem. Soc. Faraday Trans. 1 Phys. Chem. Condens Ph. 83 (1987) 3271–3282, https://doi.org/10.1039/F19878303271.
- [52] M. Fleischmann, K. Korinek, D. Pletcher, The oxidation of hydrazine at a nickel anode in alkaline solution, J. Electroanal. Chem. 34 (1972) 499–503, https://doi. org/10.1016/S0022-0728(72)80425-X.
- [53] T. Sakamoto, H. Kishi, S. Yamaguchi, D. Matsumura, K. Tamura, A. Hori, Y. Horiuchi, A. Serov, K. Artyushkova, P. Atanassov, H. Tanaka, Mechanism study of hydrazine electrooxidation reaction on nickel oxide surface in alkaline electrolyte by *In situ* XAFS, J. Electrochem. Soc. 163 (2016) H951–H957, https:// doi.org/10.1149/2.0571610jes.
- [54] K. Rajendran, D. Jagadeesan, Harnessing the oxygen vacancies in metal oxides for nitroreduction, ChemCatChem 16 (2024) 2–6, https://doi.org/10.1002/ cctc.202301647.